Maximum heat transfer density rate enhancement from cylinders rotating in natural convection

L. G. Page[a], T. Bello-Ochende[a,*], J. P. Meyer[a]

[a] Department of Mechanical and Aeronautical Engineering, University of Pretoria, Pretoria, Private Bag X20, Hatfield, 0028, South Africa.

Abstract

In this paper we investigate the thermal behaviour of an assembly of consecutive cylinders in a counter-rotating configuration cooled by natural convection with the objective of maximizing the heat transfer density rate (heat transfer rate per unit volume). A numerical model is used to solve the governing equations that describe the temperature and flow fields. The spacing between the consecutive cylinders is optimised for each flow regime (Rayleigh number) and cylinder rotation speed. It was found that the optimized spacing decreases as the Rayleigh number increases and the heat transfer density rate increases, for the optimized structure, as the cylinder rotation speed is increased. Results further shows that there is an increase in the heat transfer density rate of the rotating cylinders over stationary cylinders.

Keywords: Natural convection; Rotating cylinders; Heat transfer density rate; Counter-rotation; Optimal packing

Nomenclature

D_o	cylinder diameter, m
g	gravitational acceleration, $\mathrm{m/s^2}$
H_d	downstream flow length, m
H_u	upstream flow length, m
k	thermal conductivity, $\mathrm{W/mK}$
L	assembly length, m
P	pressure, Pa
Pr	Prandtl number

*Corresponding author. Tel.: +27 (012) 420 3105; Fax: +27 (012) 362 5124

E-mail address: Tunde.Bello-Ochende@up.ac.za (T. Bello-Ochende).

$\tilde{q}$	dimensionless heat transfer density rate
q	total heat transfer rate, W
q'	heat transfer rate per unit length, $\mathrm{W/m}$
q''	heat transfer rate per unit area, $\mathrm{W/m^2}$
q'''	heat transfer density rate, $\mathrm{W/m^3}$
Ra	Rayleigh number
S_o	spacing between cylinders, m
T	temperature, K
T_w	wall temperature, K
T_∞	inlet fluid temperature, K
U	velocity vector, $\mathrm{m/s}$
(u, v, w)	velocity components, $\mathrm{m/s}$
(x, y)	Cartesian coordinates, m

Greek symbols

α	thermal diffusivity, $\mathrm{m^2/s}$
β	thermal expansion coefficient, $1/\mathrm{K}$
μ	viscosity, $\mathrm{kg/ms}$
δ_T	thermal boundary layer thickness, m
ν	kinematic viscosity, $\mathrm{m^2/s}$
ρ	density, $\mathrm{kg/m^3}$
ω_o	cylinder angular velocity, $\mathrm{rad/s}$

Subscripts

m	maximum
opt	optimum

Superscripts

~	dimensionless variables

^ unit vector

1. Introduction

Efficiency is a key aspect in design, which has become prevalent in the design of heat transfer devices such as heat sinks and pin fins. Research has been and is still being conducted on this subject with the aim of extracting more and more heat from a given space through the maximizing of the packing of heat-generating material per unit volume. This drive to augment heat transfer devices has become reinforced by modern electronic systems which produce high amounts of heat due to the ever increasing power-to-volume ratio employed in such systems.

The strive for greater heat transfer density rates has been the driving force behind many of the miniaturization efforts, augmentations and unconventional ways of designing heat transfer devices. This has lead researchers to study the optimized configurations for various architectures such as: the optimal spacing of parallel plates in forced convection, natural convection and mixed convection [1-4]; the optimal spacing of cylinders in forced convection and natural convection [5, 6]; and various optimized multi-scale structures [7-12], etc.

The heat transfer and fluid flow around a single rotating cylinder has been studied previously. Badr and Dennis [13] considered the problem of laminar forced convective heat transfer from an isothermal circular cylinder rotating about its own axis located in a uniform stream. The authors reported that the temperature fields are strongly influenced by the rotational speed of the cylinder and contradictory to expectation they found that the overall heat transfer coefficient tends to decrease as the rotational of the cylinder increases. They attributed this to the presences of a rotating fluid layer around the cylinder that separates the cylinder from the main flow stream. Chiou and Lee [14] considered a problem of forced convection on a rotating cylinder cooled with an air jet. The results confirmed that the overall heat transfer is enhanced at lower rotational speeds and at higher rotational speeds the effect became reversed. They attributed this to the presences of a layer of dead air around the cylinder. Panda and Chhabra [15] considered a problem of forced convection heat transfer from a heated cylinder rotating in streaming power-law fluids. The results show a similar behaviour of the heat transfer rate: for moderate rotational velocities at low Reynolds numbers the heat transfer rate is enhanced and there is an envelope of conditions (Reynolds number, rotation speed and power-law index) in which rotation has a negative effect on the heat transfer rate. Similar research includes the works of Gshwendtner [16], Mohanty et al. [17], Oesterle et al. [18], Ozerdem [19], Paramane and Sharma [20,21], Yan and Zu [22] and Nobari et al. [23].

Further studies have been conducted with a row of heat-generating rotating cylinders in forced

convection by Joucaviel et al. [24]. Here the authors report that a counter-rotation configuration increases the heat transfer more efficiently when compared to a co-rotation configuration. Ogunronbi et al. [25] then built onto this work as well as prior research by Bello-Ochende and Bejan [10] by considering a multi-scale constructal design. The study presented in this paper builds onto prior research by Bello-Ochende and Bejan [12], in which the authors optimized the cylinder-to-cylinder spacings in a multi-scale constructal design of heat-generating cylinders (without cylinder rotation) cooled by natural convection for one and two degrees of freedom. These classical results will be used as a reference (benchmark) for the results reported in this paper. It is the purpose of this paper to maximize the heat transfer density rate of a row of heat-generating rotating cylinders in steady laminar single-phase natural convection. The assembly of cylinders rotate in a counter-rotating configuration.

2. Model

Consider a row of infinity long, rotating and heat-generating parallel cylinders aligned along a single line to form a stacking as shown in Fig. 1. The cylinders rotate at an angular velocity of ω_o in a counter-rotating configuration. The cylinder diameter (D_o) is fixed and the surface temperature of the cylinders (T_w) is assumed uniform and constant and greater than that of the fluid temperature (T_∞). The cylinders are cooled by natural convection. The objective is to select the number of cylinders in the stacking or the cylinder-to-cylinder spacing (S_o) in such a manner that the overall thermal heat transfer between the cylinders and the ambient air is maximized. This is done for each flow regime (Rayleigh number) and cylinder rotation speed. The flow is assumed steady, laminar, incompressible and two-dimensional. All thermophysical properties are assumed constant. The temperature variations are assumed sufficiently small relative to the absolute temperature so that the Boussinesq approximation is valid.

Figure 2 shows the elemental volume that characterises this assembly. The computational domain comprises of the upstream section $[H_u \times 2(D_o + S_o)]$, the downstream section $[H_d \times 2(D_o + S_o)]$ and the flow region $[(D_o \times 2(D_o + S_o)]$. The upstream lengths ($H_u$) and downstream lengths (H_d) were selected based on mesh independency tests described in section 3. The conservation equations (in vector form) for mass, momentum and energy are respectively:

$$\nabla U = 0 \tag{1}$$

$$(U \cdot \nabla U) = -\frac{1}{\rho}\nabla P + \nu \nabla^2 U + g\beta(T - T_\infty)\hat{k} \tag{2}$$

$$(U \cdot \nabla T) = \alpha \nabla^2 T \tag{3}$$

Where $U = [u \quad v \quad w]^T$ is the velocity field, $\hat{k} = [0 \quad 1 \quad 0]^T$ is a unit vector indicating the direction in which gravity acts and $\nabla^2 = \partial^2/\partial x^2 + \partial^2/\partial y^2 + \partial^2/\partial z^2$.

The system of coordinates (x, y) and the velocity component (u, v) are defined in Fig. 2. The variables are defined in the nomenclature. The numerical work of solving Eqs. (1) to (3) is based on dimensionless formulation using the variables:

$$\tilde{x}, \tilde{y}, \tilde{z} = \frac{(x,y,z)}{D_o}, \qquad \tilde{u}, \tilde{v}, \tilde{w} = \frac{(u, v, w)}{(\alpha/D_o)(Ra_{D_o}\ Pr)^{1/2}} \tag{4}$$

$$\tilde{T} = \frac{T-T_\infty}{T_w-T_\infty}, \qquad \tilde{P} = \frac{P}{(\alpha\mu / D_o^{\,2})(Ra_{D_o}\ Pr)^{1/2}} \tag{5}$$

$$\tilde{\omega}_o = \frac{\omega_o}{(2\alpha/D_o^{\,2})(Ra_{D_o}\ Pr)^{1/2}} \tag{6}$$

Where the Prandtl number is $Pr = \nu/\alpha$ and the Rayleigh number is defined in terms of the cylinder diameter,

$$Ra = \frac{g\beta(T_w - T_\infty)D_o^{\,3}}{\alpha\nu} \tag{7}$$

Substituting Eqs. (4) to (7) into Eqs. (1) to (3) yields the dimensionless version of the mass, momentum and energy equations respectively:

$$\tilde{\nabla}\tilde{U} = 0 \tag{8}$$

$$\left(\frac{Ra}{Pr}\right)^{1/2}(\tilde{U}\cdot\nabla\tilde{U}) = -\tilde{\nabla}\tilde{P} + \tilde{\nabla}^2\tilde{U} + \left(\frac{Ra}{Pr}\right)^{1/2}\tilde{T}\hat{k} \tag{9}$$

$$\left(\frac{Ra}{Pr}\right)^{1/2}(\tilde{U}\cdot\nabla\tilde{T}) = \tilde{\nabla}^2\tilde{T} \tag{10}$$

Where $\tilde{U} = [\tilde{u} \quad \tilde{v} \quad \tilde{w}]^T$ is the dimensionless velocity field. All geometric dimensions (cylinder diameter, cylinder-to-cylinder spacing, upstream and downstream lengths) of the computational domain, shown in Fig. 2, were also made dimensionless:

$$\tilde{D}_o = \frac{D_o}{D_o} = 1, \qquad \tilde{S}_o = \frac{S_o}{D_o} \qquad \tilde{H}_u, \tilde{H}_u = \frac{H_u, H_d}{D_o} \tag{11}$$

The flow boundary conditions are indicated in Fig. 2. For the cylinder surfaces, the boundary conditions are specified as zero slip, zero penetration, constant uniform surface temperature $\tilde{T}_w = 1$ and an angular velocity of $\tilde{\omega}_o$. For the inlet of the computational domain, the boundary

conditions are specified as $\tilde{P} = 0$, $\tilde{T}_\infty = 0$ and $\tilde{u} = \partial\tilde{v}/\partial\tilde{y} = 0$. For the exit of the computational domain, the boundary conditions are specified as $\partial(\tilde{u}, \tilde{v})/\partial\tilde{y} = 0$, $\partial\tilde{P}/\partial\tilde{y} = 0$ and $\partial\tilde{T}/\partial\tilde{y} = 0$. For the upstream section ($0 \le \tilde{y} \le \tilde{\mathrm{H}}_u$) of the computational domain, the boundary conditions are specified as symmetry planes or free slip and no penetration ($\tilde{u} = \partial(\tilde{v}, \tilde{T})/\partial\tilde{x} = 0$). For the downstream section ($\tilde{\mathrm{H}}_u \le \tilde{y} \le \tilde{\mathrm{H}}_u + \tilde{\mathrm{D}}_o + \tilde{\mathrm{H}}_d$) of the computational domain, two boundary conditions are specified: symmetry plane or free slip and no penetration ($\tilde{u} = \partial(\tilde{v}, \tilde{T})/\partial\tilde{x} = 0$) at the left side of the flow region and; zero stress ($\partial\tilde{P}/\partial\tilde{x} = 0$ and $\partial\tilde{u}/\partial\tilde{x} = \partial(\tilde{v}, \tilde{T})/\partial\tilde{x} = 0$) on the right side of the flow region. By specifying $\partial\tilde{u}/\partial\tilde{x} = 0$ on the right side of the flow region, fluid is allowed to flow horizontally into the computational domain. This entrainment effect nullifies the unrealistic vertical acceleration or chimney effect that would have been generated had we specified zero slip on this side.

The cylinder-to-cylinder spacing is varied and thus we are interested in the geometric configuration that maximizes the overall heat transfer between the cylinders and the surrounding fluid. The dimensionless quantity used to evaluate this configuration is the dimensionless heat transfer density rate. The heat transfer density rate is $q''' = q'/2D_o(D_o + S_o)$, where q' is the sum of the total heat transfer rate integrated over the surface of the cylinders:

$$q' = \sum_{i=1}^{2} \int_0^{2\pi} k(-\nabla T)_n d\theta \tag{12}$$

Where the subscript n denotes that gradient of T is taken with respects to the normal direction to the cylinder surface. The corresponding dimensionless heat transfer density rate is:

$$\tilde{q} = \frac{q'}{D_o(D_o + S_o)k(T_w - T_\infty)} \tag{13}$$

3. Numerical method

Equations (8) to (10) were solved using a finite volume code [26], with hexahedron elements. The velocity-pressure coupled equations were solved using the Semi-Implicit Method for Pressure-Linked Equations (SIMPLE) algorithm [27]. The derivative terms in these equations were solved using the Gaussian finite volume integration for the discretisation scheme with the interpolation schemes specified as: central differencing for the gradient term; upwind differencing for the divergence term; and central differencing with unbounded, second order, conservative numerical behaviour for the Laplacian term. The computational fluid dynamic code [28] solves the steady-state Eqs. (8) to (10) by introducing a non-zero time derivative (dummy time variable). Thus the steady-state problem is viewed as a transient problem with an infinite time step.

The convergence criteria at each time step were

$$\frac{\left\|\tilde{U}_t^{(k)} - \tilde{U}_t^{(k-1)}\right\|}{\left\|\tilde{U}_t^{(k)}\right\|} \leq 10^{-4} \text{ and } \frac{\left\|\tilde{T}_t^{(k)} - \tilde{T}_t^{(k-1)}\right\|}{\left\|\tilde{T}_t^{(k)}\right\|} \leq 10^{-6} \tag{14}$$

And the convergence criteria to terminate the time step was

$$\frac{\left\|\tilde{q}_t - \tilde{q}_{t-1}\right\|}{\left\|\tilde{q}_t\right\|} \leq 10^{-3} \tag{15}$$

In which k is the iteration counter, t is the time step counter and $\|\bullet\|$ is the Euclidean norm.

The mesh design received special attention and was tested extensively in the range $10^1 \leqslant Ra \leqslant 10^4$ with the grid varying from one geometric configuration to the next. The mesh was uniform in the $\tilde{x}$ direction and double graded in the $\tilde{y}$ direction so as to put more elements near the cylinder surfaces to more accurately capture the behaviour of the boundary layers. The initial guess for the mesh size in the $\tilde{x}$ direction was chosen based on the boundary layer thickness scale $\delta_T \sim D_o Ra^{(-1/4)}$. Table 1 (a) shows the mesh refinement summary for the number of nodes for the range $10^1 \leqslant Ra \leqslant 10^4$. For example the mesh refinement study shows, for $Ra = 10^1$, the heat transfer density rate is insensitive (varies by less than 1%) to further mesh refinement when 16 elements per unit length were used. Table 1 (b) shows one example of how mesh independence was achieved for $Ra = 10^3$, $\tilde{S}_o = 0.3$ and $Pr = 0.71$. Table 1 (c) shows the grid refinement study for the upstream and downstream lengths. For example the grid refinement study shows for $Ra = 10^2$, when $\tilde{H}_u = 1.5$ and $\tilde{H}_d = 2.5$, the heat transfer density rate is insensitive to further doubling of upstream and downstream lengths.

4. Numerical results and scale analysis

The flow and temperature fields were simulated in a large number of configurations, in order to determine the effect of the cylinder-to-cylinder spacing on the heat transfer density rate at each flow regime for each cylinder rotation speed. The Rayleigh number range considered is $10^1 \leqslant Ra \leqslant 10^4$ and the cylinder rotation speed range considered is $0 \leqslant \tilde{\omega}_o \leqslant 10$. The optimal packing in Fig. 1 is achieved when the cylinder-to-cylinder spacing is such that the thermal boundary layers of the cylinders just touch. According to scale analysis, the thermal boundary layer of a cylinder with laminar natural convection flow and $Pr \sim 1$ [29] has a thickness of order:

$$\delta_T \sim D_o Ra^{(-1/4)} \tag{16}$$

By setting the thermal boundary layer thickness, $\delta_T \sim 2S_o$ in Eq. (16), we find that:

$$\tilde{S}_{o,opt} \sim 2Ra^{(-1/4)} \tag{17}$$

The heat transfer density rate can be analysed based on the same scaling argument. The cylinder heat flux (heat transfer rate per unit area) scale is $q'' \sim \mathrm{k}\,(T_w - T_\infty)/\delta_T$, where $\delta_T \sim D_o Ra^{(-1/4)}$. Because $S_o < D_o$, cf. Eq. (16) for $Ra \gg 1$, the heat transfer density rate is $q''' \sim q''/D_o$, such that the dimensionless heat transfer density rate becomes:

$$\tilde{q} \sim \frac{q'''D_o^{\,2}}{k(T_w\text{-}T_\infty)} \sim Ra^{(1/4)} \tag{18}$$

4.1. Stationary cylinders

Figure 3 shows that the heat transfer density rate is optimal when $\tilde{S}_o$ has a certain value, when there is no cylinder rotation. The optimal spacing, shown in Fig. 3, for $Ra = 10^3$, $Pr = 0.71$ and $\tilde{\omega}_o = 0$ is $\tilde{S}_{o,opt} = 0.291$. There is a 0.6% difference when comparing this optimal spacing with that reported in Ref. [12] for a single row of cylinders. The optimal cylinder-to-cylinder spacings and corresponding maximum heat transfer density rates for $10^1 \leqslant Ra \leqslant 10^4$, $Pr = 0.71$ and $\tilde{\omega}_o = 0$ are summarized in Fig. 4. In this figure, the optimal cylinder-to-cylinder spacings can be correlated by the power law, within 0.25%:

$$\tilde{S}_{o,opt} = 1.76Ra^{-0.26} \tag{19}$$

Equation (19) is anticipated well by the scale analysis argument, cf. Eq. (17). This correlation also compares well with the power law correlation proposed by Ref. [12]: $\tilde{S}_{o,opt} = 1.32Ra^{-0.22}$ for $10^3 \leqslant Ra \leqslant 10^5$, there is a 1% difference ($Ra = 10^3$), 8% difference ($Ra = 10^4$) and 16% difference ($Ra = 10^5$).

The corresponding maximum heat transfer density rates, reported in Fig. 4, can be correlated by the power law, within 0.05%:

$$\tilde{q}_m = 0.72Ra^{0.29} \tag{20}$$

Again Eq. (20) is anticipated well by the scale analysis argument, cf. Eq. (18). This correlation also compares well with the power law correlation proposed by Ref. [12]: $\tilde{q}_m = 0.65Ra^{0.30}$ for $10^3 \leqslant Ra \leqslant 10^5$, there is a 3% difference ($Ra = 10^3$), 1% difference ($Ra = 10^4$) and 1% difference ($Ra = 10^5$).

4.2. Rotating cylinders

Figure 5 shows the optimal cylinder-to-cylinder spacing and the heat transfer density rate for $Ra = 10^1$ and $Pr = 0.71$ at different cylinder rotation speeds ($0 \leqslant \tilde{\omega}_o \leqslant 10$). The optimal cyl-

inder-to-cylinder spacing decreases and the maximum heat transfer density rate increases as the cylinder rotational speed is increased. There is a 63% increase in the maximum heat transfer density rate for the optimized structure when the cylinder rotation speed is increased from stationary to $\widetilde{\omega}_o = 10$.

The optimal cylinder-to-cylinder spacings for $10^1 \leqslant Ra \leqslant 10^4$, $Pr = 0.71$ and $0 \leqslant \widetilde{\omega}_o \leqslant 10$ are summarized in Fig. 6. A cylinder rotational speed of $\widetilde{\omega}_o = 0.01$ has no impact on the optimal cylinder-to-cylinder spacing when compared to that of stationary cylinders. The optimal cylinder-to-cylinder spacing is reduced by 3.5% for $Ra = 10^4$ and by less than 1.5% for $10^1 \leqslant Ra \leqslant 10^3$ when the cylinder rotational speed is increased from stationary to $\widetilde{\omega}_o = 0.1$. There is a 57% decrease in the optimal cylinder-to-cylinder spacing for $Ra = 10^2$ when the cylinder rotation speed is increased from stationary to $\widetilde{\omega}_o = 10$ and a 17% decrease in the optimal cylinder-to-cylinder spacing for $Ra = 10^3$ when the cylinder rotation speed is increased from stationary to $\widetilde{\omega}_o = 1$.

When the Rayleigh number is equal to 10^3 and the cylinder rotational speed is greater than 1, the results become non-physical because the laminar model of the flow collapses due to a wake and consequent turbulence, which dominates the flow behind the rotating cylinders. This is also the case for when the Rayleigh number is equal to 10^4 and the cylinder rotational speed is greater than 0.1.

The optimal cylinder-to-cylinder spacings, reported in Fig. 6, can be correlated by a power law, within 0.33%, of the form $\tilde{S}_{o.opt} = CRa^n$ where C is equal to 1.77, 1.75, 1.65, 1.27 and n is equal to -0.27, -0.27, -0.27, -0.37 for the cylinder rotation speeds 0.01, 0.1, 1 and 10 respectively. These individual correlations can be simplified into one power law correlation, with an error of less than 1%:

$$\tilde{S}_{o.opt} = -0.05{\widetilde{\omega}_o}^{0.86} + 1.69Ra^{-0.25} \tag{21}$$

The maximum heat transfer density rates for $10^1 \leqslant Ra \leqslant 10^4$, $Pr = 0.71$ and $0 \leqslant \widetilde{\omega}_o \leqslant 10$ are summarized in Fig. 7. A cylinder rotational speed of $\widetilde{\omega}_o = 0.01$ has less than a 0.4% increase on the maximum heat transfer density rate when compared to that of stationary cylinders. The maximum heat transfer density rate is increase by 2.5% for $Ra = 10^4$ and by less than 1.5% for $10^1 \leqslant Ra \leqslant 10^3$ when the cylinder rotational speed is increased from stationary to $\widetilde{\omega}_o = 0.1$. There is a 46% increase in the maximum heat transfer density rate for $Ra = 10^2$ when the cylinder rotation speed is increased from stationary to $\widetilde{\omega}_o = 10$ and a 13% increase in the maximum heat transfer density rate for $Ra = 10^3$ when the cylinder rotation speed is increased from stationary to $\widetilde{\omega}_o = 1$.

The maximum heat transfer density rates, reported in Fig. 7, can be correlated by a power law, within 0.05%, of the form $\tilde{q}_m = CRa^n$ where C is equal to 0.72, 0.72, 0.70, 1.22 and n is equal to 0.29, 0.29, 0.31, 0.25 for the cylinder rotation speeds 0.01, 0.1, 1 and 10 respectively. Again these individual correlations can be simplified into one power law correlation, with an error of less than 1%:

$$\tilde{q}_m = 0.32\tilde{\omega}_o{}^{0.49} + 0.71Ra^{0.29} \tag{22}$$

Figure 8 shows the effect of cylinder rotational speed on the thermal boundary layer for a row of rotating cylinders shown in Fig. 1 for $Ra = 10^2$, $Pr = 0.71$ and $\tilde{S}_o = 0.5$. Fig. 8 (a) shows, for $\tilde{\omega}_o = 0$, that the thermal boundary layer between two consecutive cylinders touches near the centreline of the cylinders. Fig. 8 (b) shows, for $\tilde{\omega}_o = 10$, that the thermal boundary layer between two consecutive cylinders (where the cylinder rotation aids the flow direction) is extended and touches just past the top of the cylinders. Similarly, the thermal boundary layer between two consecutive cylinders (where the cylinder rotation opposes the flow direction) remains relatively unchanged.

In Fig. 9 we drew to scale the optimized flow configuration for $Ra = 10^1$ and $Pr = 0.71$ for a cylinder rotation speed of (a) $\tilde{\omega}_o = 0$ and (b) $\tilde{\omega}_o = 10$. The addition of rotation to the cylinders serves to maximize the packing (minimize the cylinder-to-cylinder spacing) of heat generating cylinders.

5. Conclusions

In this paper we showed numerically the effect of counter-rotation on a row of heat-generating cylinders which were cooled by natural convection. The cylinder-to-cylinder spacing was optimized for each flow regime and rotational speed on the cylinders. In the Rayleigh number range considered it was shown that the maximum heat transfer density rate increased and the optimal cylinder-to-cylinder spacing decreased with an increase in cylinder rotation speed. Thus from a heat transfer density rate point of view it is beneficial to add rotation to the cylinders. Further research may include a multi-scale constructal design or focus on a three-dimensional numerical model.

Acknowledgements

The authors acknowledge with gratitude the support from the University of Pretoria and the National Research Foundation (NRF-DST).

References

[1] A. Bejan, E. Sciubba, The optimal spacing for parallel plates cooled by forced convection, International Journal of Heat and Mass Transfer, 35 (1992) 3259–3264.

[2] A. Bejan, A.M. Morega, The optimal spacing of a stack of plates cooled by turbulent forced convection, International Journal of Heat and Mass Transfer, 37 (1994) 1045–1048.

[3] A.K. da Silva, A. Bejan, S. Lorente, Maximal heat transfer density in vertical morphing channels with natural covection, Numerical Heat Transfer Part A - Applications, 45 (2004) 135–152.

[4] T. Bello-Ochende, A. Bejan, Optimal spacings for mixed convection, Journal of Heat Transfer 126 (6) (2004) 956–962.

[5] G. Stanescu, A.J. Fowler, A. Bejan, The optimal spacing of cylinders in free-stream cross-flow forced convection, International Journal of Heat and Mass Transfer, 39 (1996) 311–317.

[6] A. Bejan, A.J. Fowler, G. Stanescu, The optimal spacing between horizontal cylinders in a fixed volume cooled by natural convection, Journal of Heat and Mass Transfer, 38 (1995) 2047–2055.

[7] A. Bejan, Y. Fautrelle, Constructal multi-scale structure for maximal heat transfer density, Acta Mechanica, 163 (2003) 39–49.

[8] T. Bello-Ochende, A. Bejan, Maximal heat transfer density: plates with multiple lengths in forced convection, International Journal of Thermal Sciences, 43 (2004) 1181–1186.

[9] A.K. da Silva, A. Bejan, Constuctal multi-scale structure for maximal heat transfer density in natural convection, International Journal of Heat and Fluid Flow, 26 (2005) 34–44.

[10] T. Bello-Ochende, A. Bejan, Constructal multi-scale cylinders in cross-flow, International Journal of Heat and Mass Transfer, 48 (2005) 1373–1383.

[11] T. Bello-Ochende, J.P. Meyer, J. Dirker, Three-dimensional multi-scale plate assembly for maximum heat transfer rate density, International Journal of Heat and Mass Transfer, 53 (2010) 586–593.

[12] T. Bello-Ochende, A. Bejan, Constructal multi-scale cylinders with natural convection, International Journal of Heat and Mass Transfer, 48 (2005) 4300–4306.

[13] H.M. Badr, S.C.R. Dennis, Laminar forced convection from a rotating cylinder, International Journal of Heat and Mass Transfer, 28 (1985) 253–264.

[14] C.C. Chiou, S.L. Lee, Forced convection on a rotating cylinder with an incident air jet, International Journal of Heat and Mass Transfer, 36 (1993) 3841-3850.

[15] S.K. Panda, R.P. Chhabra, Laminar forced convection heat transfer from a rotating cylinder to power-law fluids, Numerical Heat Transfer; Part A: Applications, 59 (4) (2011) 297–319

[16] M.A. Gshwendtner, Optical investigation of the heat transfer from a rotating cylinder in a cross flow, Heat and Mass Transfer, 40 (2004) 561–572.

[17] A. K. Mohanty, A.A. Tawfek, B.V.S.S.S. Prasad, Heat Transfer from a Rotating Cylinder in Crossflow, Experimental Thermal and Fluid Science, 10 (1995) 54–61.

[18] M. Oesterle, M. Lauster, R. Waibel, V. Lippig, D. Straub, Topological structures near a heated rotating cylinders, Experiments in Fluids, 24 (4) (1998) 308–322.

[19] B. Ozerdem, Measurement of convective heat transfer coefficient for a horizontal cylinder rotating in quiescent air, International Communications in Heat and Mass Transfer, 27 (2000) 389–395.

[20] S.B. Paramane, A. Sharma, Numerical investigation of heat and fluid flow across a rotating circular cylinder maintained at constant temperature in 2-D laminar flow regime, International Journal of Heat and Mass Transfer, 52 (2009) 3205–3216.

[21] S.B. Paramane, A. Sharma, Heat and fluid flow across a rotating cylinder dissipating uniform heat flux in 2D laminar flow regime, International Journal of Heat and Mass Transfer, 53 (2010) 4672–4683.

[22] Y.Y. Yan, Y.Q. Zu, Numerical simulation of heat transfer and fluid flow past a rotating isothermal cylinder – a LBM approach, International Journal of Heat and Mass Transfer, 51 (2008) 2519–2536.

[23] M.R.H. Nobari, K. Gharali, M. Tajdari, A numerical study of flow and heat transfer in internally finned rotating curved pipes, Numerical Heat Transfer; Part A: Applications, 56 (1) (2009) 76–95

[24] M. Joucaviel, L. Gosselin, T. Bello-Ochende, Maximum heat transfer density with rotating cylinders aligned in cross-flow, International Communications in Heat and Mass Transfer, 35 (2008) 557–564.

[25] O.I. Ogunronbi, T. Bello-Ochende, J.P. Meyer, Constructal multiscale cylinders rotating in cross-flow, International Journal of Heat and Mass Transfer, 54 (2011) 2568–2577.

[26] OpenFOAM User Guide, 21 May 2011 <http://www.openfoam.com/docs/user/>.

[27] OpenFOAM Simple Algorithm, 21 May 2011 <http://openfoamwiki.net/index.php/The_SIMPLE_algorithm_in_OpenFOAM>.

[28] OpenFOAM-1.7.1 Documentation, 21 May 2011 <http://www.openfoam.com/docs/cpp/>.

[29] A. Bejan, Convection Heat Transfer, third ed., Wiley, New York, 2004.

Figure Captions:

Fig. 1: Single row of counter-rotating cylinders in natural convection.

Fig. 2: The computational domain and boundary conditions for a set of counter-rotating cylinders.

Fig. 3: The maximization of the heat transfer density rate for the assemble shown in Fig. 1 for $Ra = 10^3$, $Pr = 0.71$ and $\widetilde{\omega}_o = 0$.

Fig. 4: The optimal cylinder-to-cylinder spacings and corresponding heat transfer density rates for a row of cylinders shown in Fig. 1 for $Pr = 0.71$, $\widetilde{\omega}_o = 0$ and $10^1 \leqslant Ra \leqslant 10^4$.

Fig. 5: The maximization of the heat transfer density rate for the cylinders shown in Fig. 1 for $Ra = 10^1$ and $Pr = 0.71$ at different cylinder rotation speeds.

Fig. 6: The optimal cylinder-to-cylinder spacings for a row of rotating cylinders shown in Fig. 1 for $Pr = 0.71$.

Fig. 7: The maximum heat transfer density rates for a row of rotating cylinders shown in Fig. 1 for $Pr = 0.71$.

Fig. 8: The effect of cylinder rotational speed on the thermal boundary layer for a row of rotating cylinders shown in Fig. 1 for $\mathrm{Ra} = 10^2$, $\mathrm{Pr} = 0.71$ and $\tilde{\mathrm{S}}_\mathrm{o} = 0.5$: (a) $\widetilde{\omega}_\mathrm{o} = 0$; and (b) $\widetilde{\omega}_\mathrm{o} = 10$.

Fig. 9: The effect of cylinder rotational speed on the cylinder-to-cylinder spacing of a row of rotating cylinders shown in Fig. 1 for $\mathrm{Ra} = 10^2$ and $\mathrm{Pr} = 0.71$: (a) $\widetilde{\omega}_\mathrm{o} = 0$; and (b) $\widetilde{\omega}_\mathrm{o} = 10$.

Table 1

(a) Mesh refinement summary: Number of elements per unit length at each Rayleigh number ($Pr = 0.71$).

Ra	$Elements/L$
10^1	*16*
10^2	*48*
10^3	*48*
10^4	*100*

(b) Mesh refinement study for $Ra = 10^3$ ($\widetilde{H}_u = 1$, $\widetilde{H}_d = 2$, $\tilde{S}_o = 0.3$ and $Pr = 0.71$).

$Elements/L$	$\tilde{q}$	$\frac{\tilde{q}^i - \tilde{q}^{i+1}}{\tilde{q}^i}$
12	*6.988*	
24	*6.035*	*0.1365*
48	*5.499*	*0.0887*
96	*5.531*	*0.0058*

(c) Grid refinement summary: Upstream and downstream lengths at each Rayleigh number ($Pr = 0.71$).

Ra	$\widetilde{\mathrm{H}}_{\mathrm{u}}$	$\widetilde{\mathrm{H}}_{\mathrm{d}}$
10^1	*1.5*	*3.5*
10^2	*1.0*	*2.5*
10^3	*1.0*	*2.0*
10^4	*0.5*	*1.5*

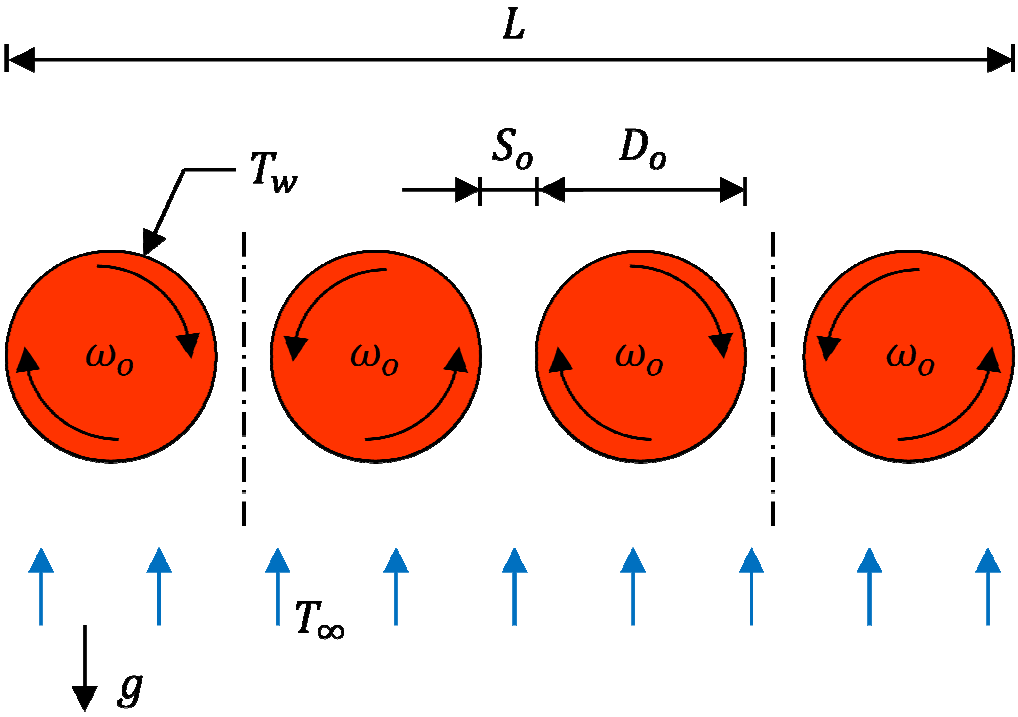

Fig. 1

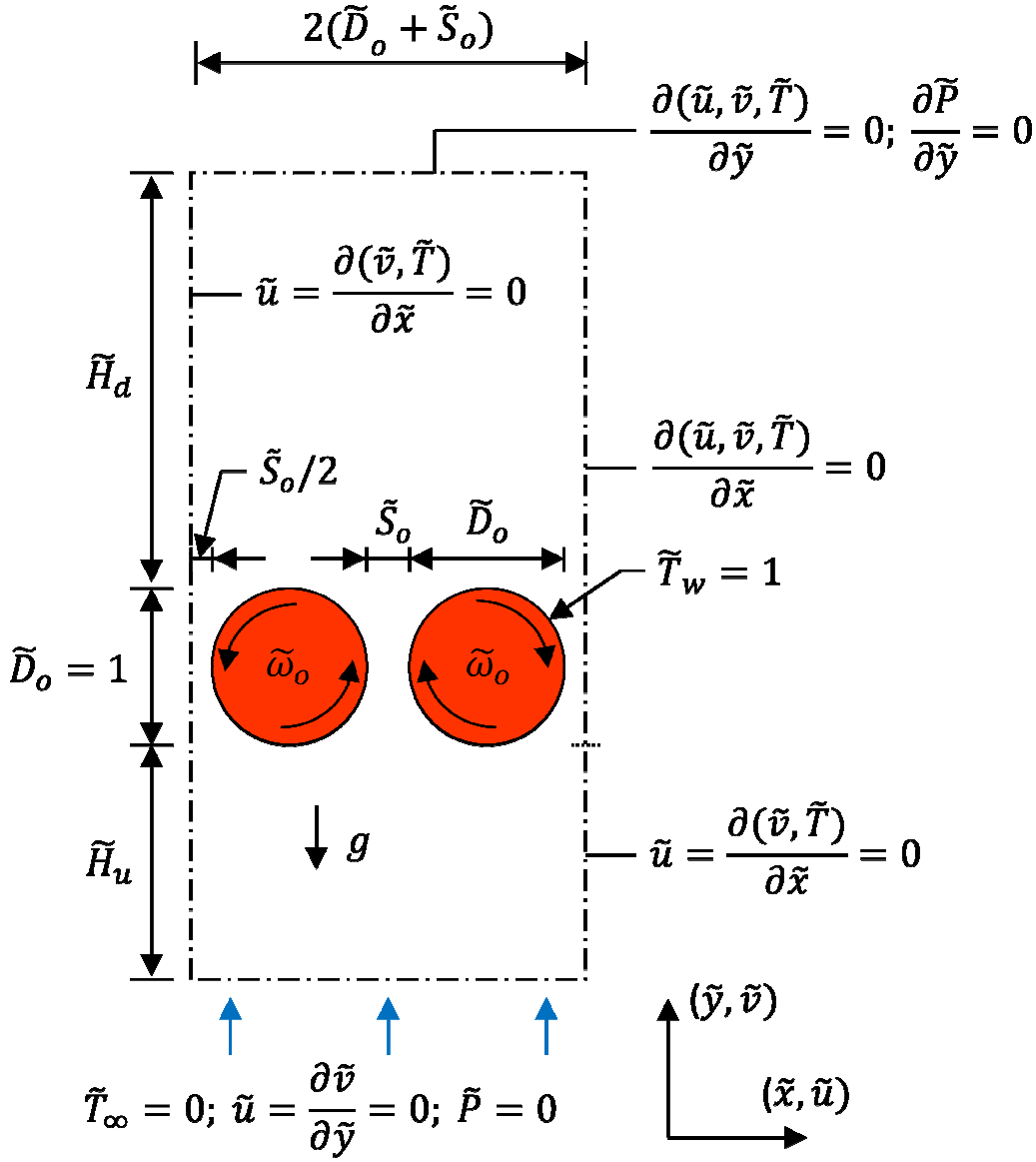
$2(\tilde{D}_o + \tilde{S}_o)$
$\frac{\partial(\tilde{u},\tilde{v},\tilde{T})}{\partial\tilde{y}} = 0;\ \frac{\partial\tilde{P}}{\partial\tilde{y}} = 0$
$\tilde{u} = \frac{\partial(\tilde{v},\tilde{T})}{\partial\tilde{x}} = 0$
$\tilde{H}_d$
$\frac{\partial(\tilde{u},\tilde{v},\tilde{T})}{\partial\tilde{x}} = 0$
$\tilde{S}_o/2$
$\tilde{S}_o$
$\tilde{D}_o$
$\tilde{T}_w = 1$
$\tilde{D}_o = 1$
$\tilde{\omega}_o$
$\tilde{\omega}_o$
g
$\tilde{H}_u$
$\tilde{u} = \frac{\partial(\tilde{v},\tilde{T})}{\partial\tilde{x}} = 0$
$(\tilde{y},\tilde{v})$
$(\tilde{x},\tilde{u})$
$\tilde{T}_\infty = 0;\ \tilde{u} = \frac{\partial\tilde{v}}{\partial\tilde{y}} = 0;\ \tilde{P} = 0$

Fig. 2

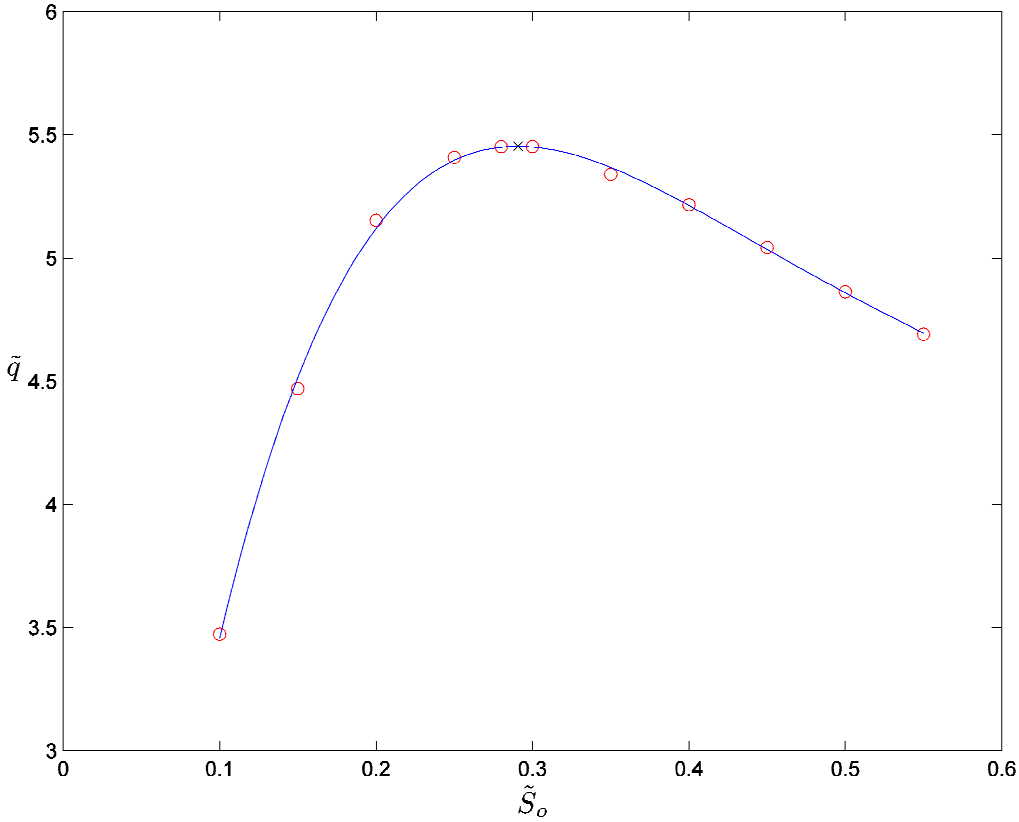

Fig. 3

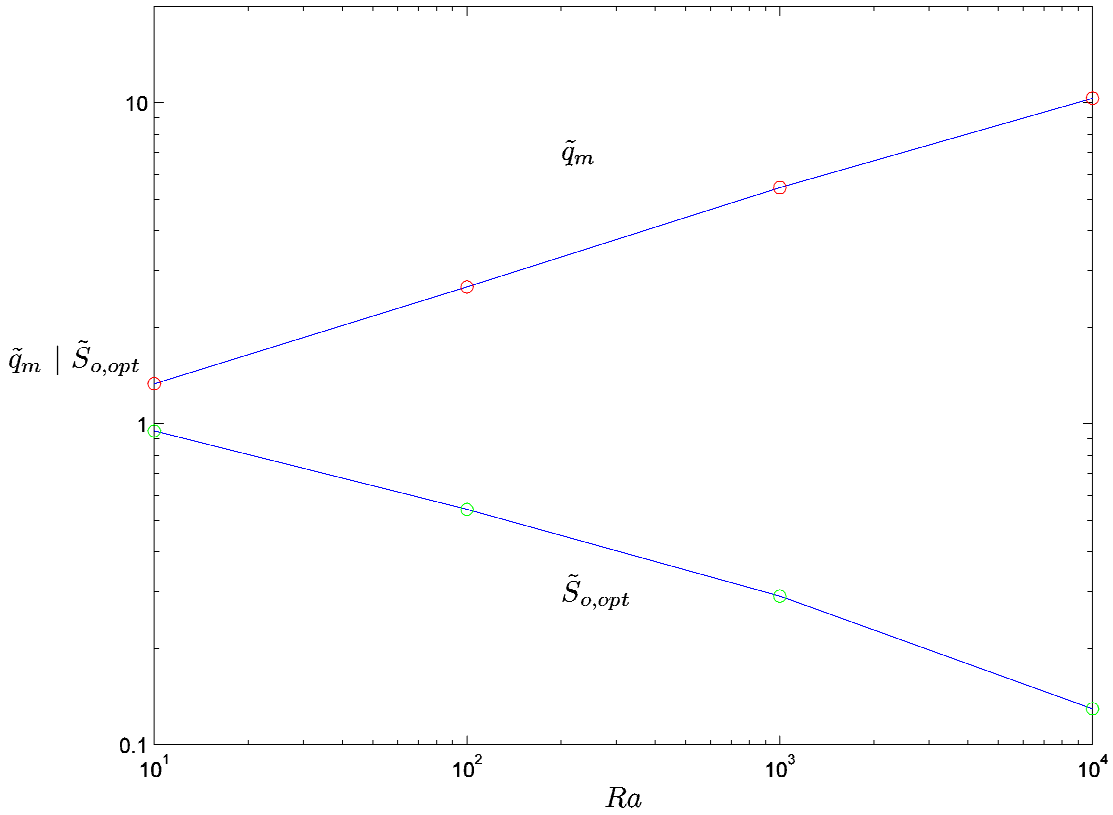
10
1
0.1
$\tilde{q}_m \mid \tilde{S}_{o,opt}$
$\tilde{q}_m$
$\tilde{S}_{o,opt}$
10^1
10^2
10^3
10^4
Ra

Fig. 4

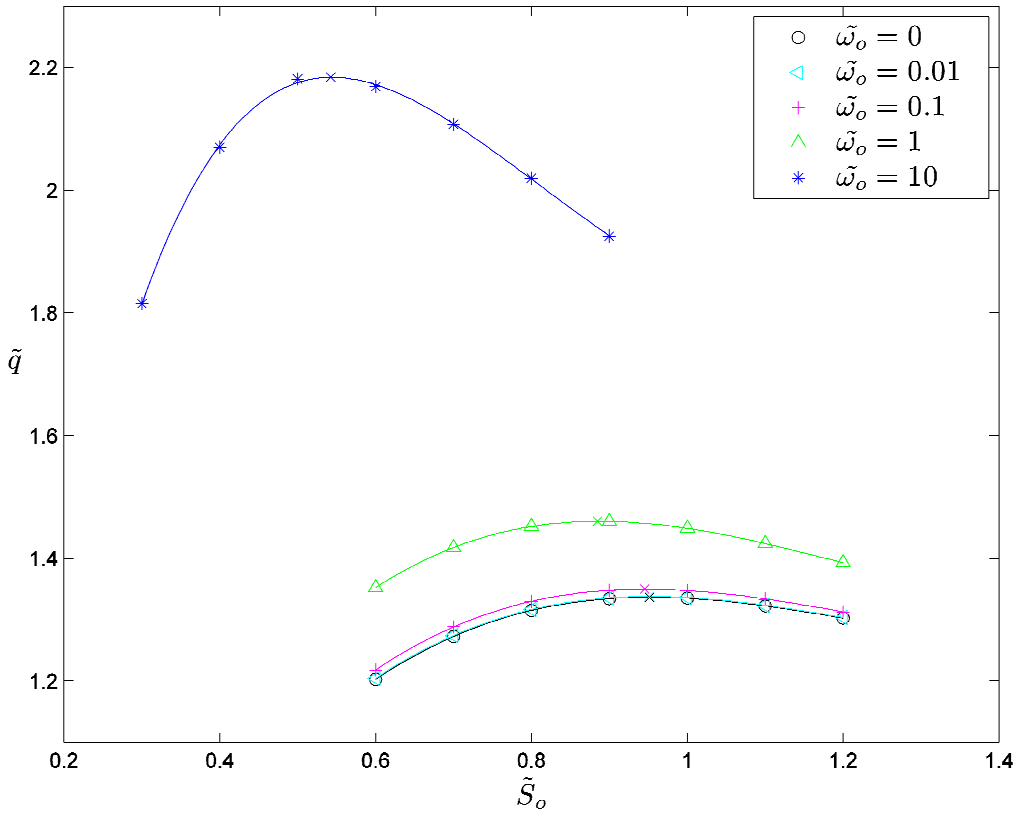
$\tilde{\omega}_o = 0$
$\tilde{\omega}_o = 0.01$
$\tilde{\omega}_o = 0.1$
$\tilde{\omega}_o = 1$
$\tilde{\omega}_o = 10$
2.2
2
1.8
1.6
1.4
1.2
$\tilde{q}$
0.2
0.4
0.6
0.8
1
1.2
1.4
$\tilde{S}_o$

Fig. 5

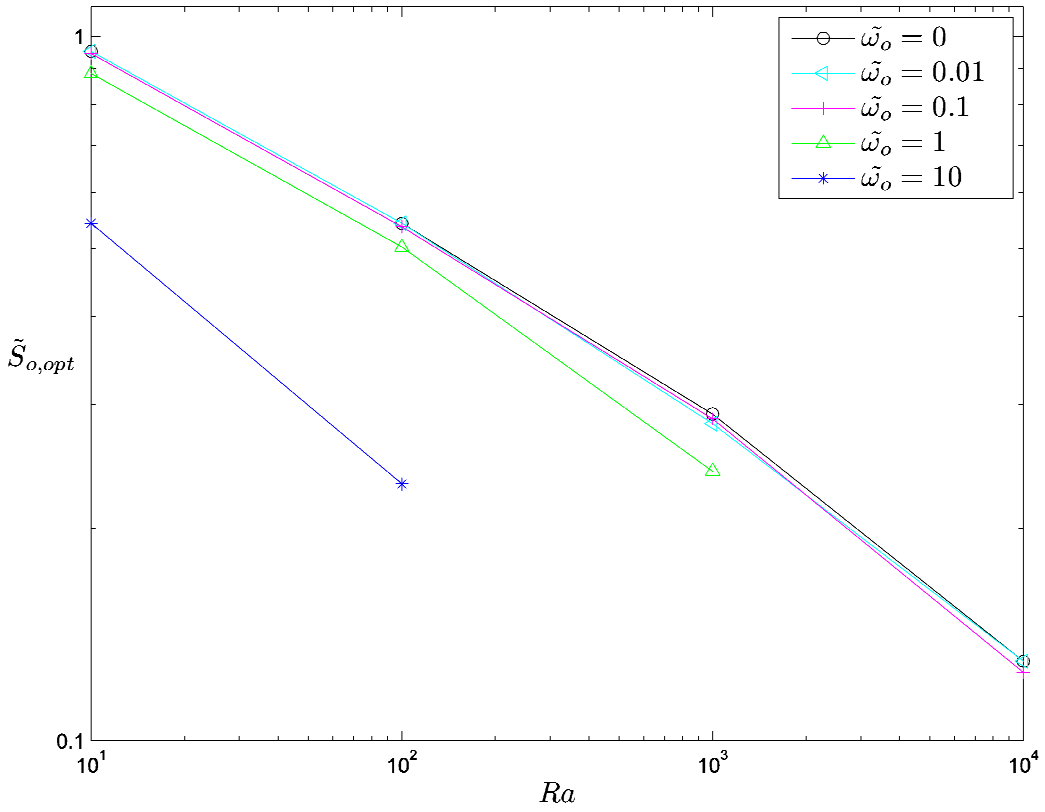
1
0.1
10^1
10^2
10^3
10^4
$\tilde{S}_{o,opt}$
Ra
$\tilde{\omega}_o = 0$
$\tilde{\omega}_o = 0.01$
$\tilde{\omega}_o = 0.1$
$\tilde{\omega}_o = 1$
$\tilde{\omega}_o = 10$

Fig. 6

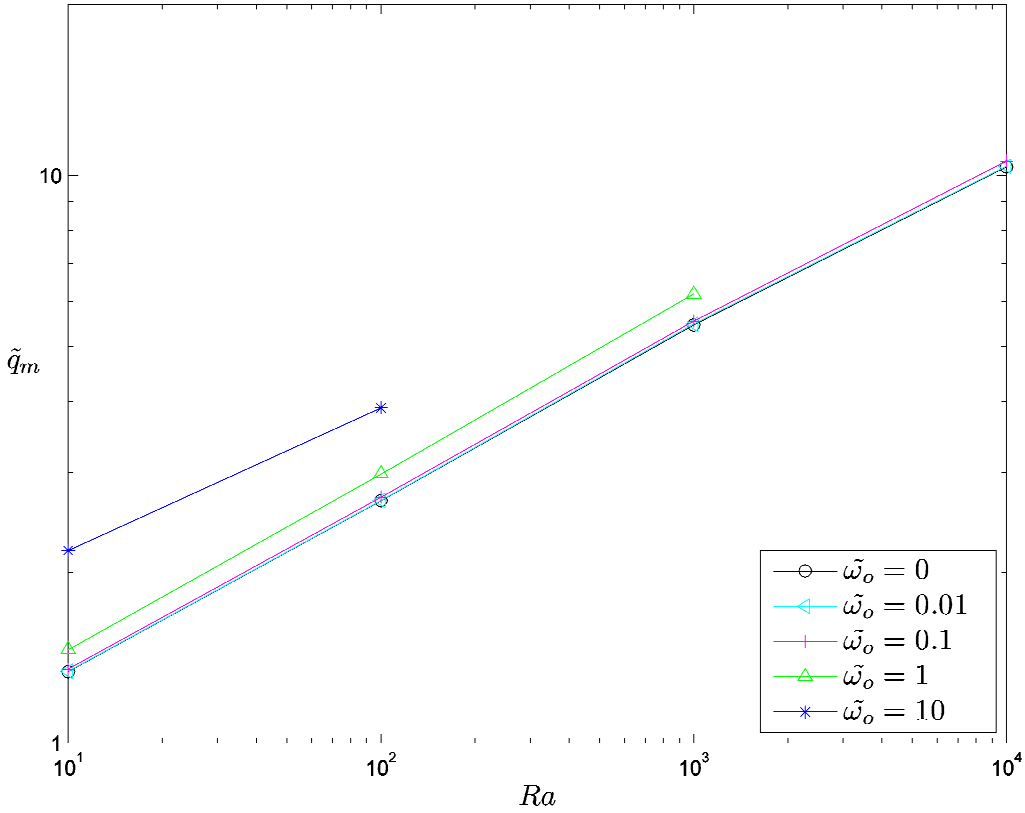
10
1
$\tilde{q}_m$
10^1
10^2
10^3
10^4
Ra
$\tilde{\omega_o} = 0$
$\tilde{\omega_o} = 0.01$
$\tilde{\omega_o} = 0.1$
$\tilde{\omega_o} = 1$
$\tilde{\omega_o} = 10$

Fig. 7

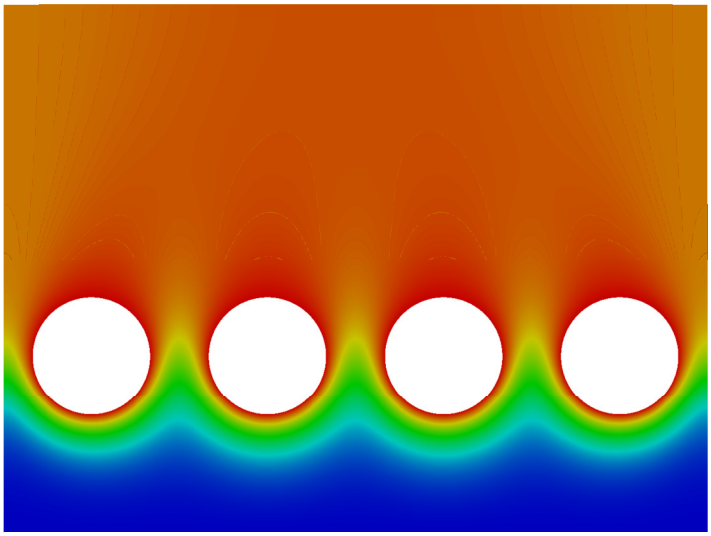

(a)

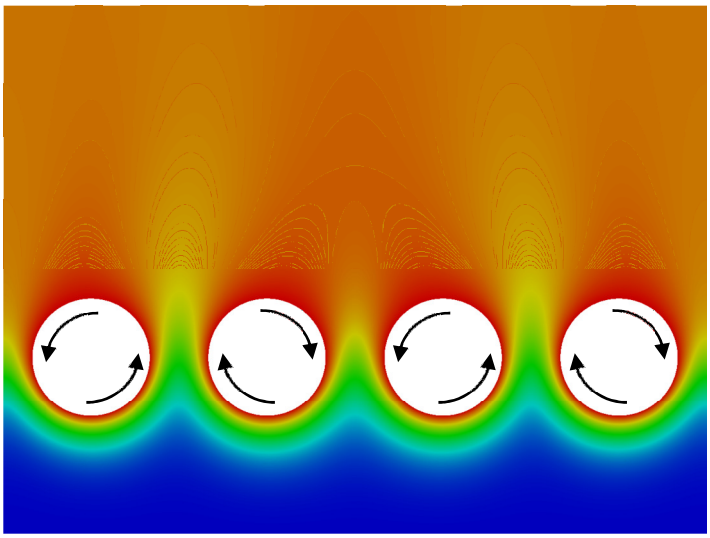

(b)

Figure 8

(a)

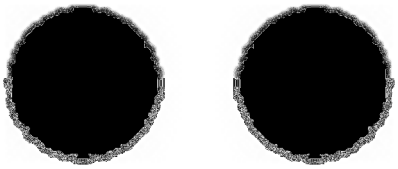

(b)

Figure 9